Original Article

Differentiation of Benign Solid Renal Lesions from Malignant Lesions Using Dual-Energy CT

Arnadda Kaewpralom MD[1], Saifhon Admontree MSc[1], Suchin Worawichawong MD[2], Pramesant Sangkum MD[3], Saowanee Srirattanapong MD[1]

[1] Department of Diagnostic and Therapeutic Radiology, Faculty of Medicine, Ramathibodi Hospital, Mahidol University, Bangkok, Thailand

[2] Department of Pathology, Faculty of Medicine Ramathibodi Hospital, Mahidol University, Bangkok, Thailand

[3] Division of Urology, Department of Surgery, Faculty of Medicine Ramathibodi Hospital, Mahidol University, Bangkok, Thailand

Objective: To evaluate the quantitative measurement of effective atomic number (Z_{eff}) and iodine density reconstructed from dual-energy computed tomography (CT) in the discrimination of malignant renal lesions from benign renal lesions.

Materials and Methods: The present study was a retrospective study that included patients with renal lesions who underwent dual-energy CT between January 2017 and June 2020. All subjects had a pathological diagnosis or follow-up imaging of at least 24 months. Two observers independently measured the Z_{eff}, iodine density, and conventional CT attenuation of the renal lesions. Associations between the different tumor types and the quantitative CT measurements reconstructed from dual-energy CT were assessed, and interobserver agreement was evaluated.

Results: Sixty-one renal lesions from 48 patients were included in the present study. No statistical differences were found in mean Z_{eff}, iodine density, or CT attenuation between the benign renal lesions and the malignant renal lesions. However, significant differences were observed in Z_{eff}, iodine density, and CT attenuation between the renal cell carcinoma (RCC) and the other malignant tumors, and between the clear cell RCC and the papillary RCC. The optimal thresholds for Z_{eff}, iodine density, and CT attenuation for distinguishing RCC from other malignant tumors were 8.22, 1.71 mg/mL, and 79.50 HU, respectively, which provided sensitivity of 76%, 76%, and 80%, respectively.

Conclusion: Benign solid renal lesions cannot be differentiated from malignant renal tumors by Z_{eff} and iodine density measurements alone. However, dual-energy Z_{eff} and iodine density have potential for the non-invasive differentiation of RCC from the other malignant renal tumors, and for the differentiation of RCC subtypes.

Keywords: Dual-energy CT; Spectral CT; Renal cell carcinoma; Renal mass; Iodine density; Effective atomic number

Received 7 December 2021 | Revised 17 March 2022 | Accepted 31 March 2022

J Med Assoc Thai 2022;105(5):413-22

Website: http://www.jmatonline.com

Renal lesions are becoming increasingly detected because of the widespread use of cross-sectional imaging[1,2]. These lesions are benign renal cysts, with 40% showing computed tomography (CT) attenuation values of less than 20 Hounsfield units (HU)[3]. When renal lesions are homogeneous with CT attenuation values of 20 to 70 HU on non-contrast-enhanced CT (NECT), or more than 20 HU on contrast-enhanced CT, differentiation between benign and malignant lesions can be difficult[4,5]. Furthermore, some types of benign solid renal tumors such as lipid-poor angiomyolipoma and oncocytoma have imaging features that overlap with those of renal cell carcinoma (RCC)[6,7], although some studies reported that the lipid-poor angiomyolipomas showed significantly higher mean attenuation values than the clear cell RCC on unenhanced scans[4,8-11], this observation is inconsistent. The management options for such tumors are active surveillance or surgical resection, and a large number of benign solid renal masses are over-treated with surgical resection[2,12,13].

According to the 2016 World Health Organization classification of adult renal tumors, RCC is the most common kidney cancer, and is classified into clear cell carcinoma at 70% to 90%, papillary carcinoma at 10% to 15%, chromophobe tumors at 3% to 5%, and collecting duct carcinoma at 1% to 2%[14]. The clear cell subtype shows a worse prognosis than the papillary or chromophobe RCC[14,15]. Most cases of RCC are detected incidentally on imaging[16].

Correspondence to:

Srirattanapong S.

Department of Diagnostic and Therapeutic Radiology, Faculty of Medicine Ramathibodi, Hospital, Mahidol University, Bangkok 10400, Thailand.

Phone: +66-81-4434233

Email: Saowanee.srr@mahidol.ac.th

How to cite this article:

Kaewpralom A, Admontree S, Worawichawong S, Sangkum P, Srirattanapong S. Differentiation of Benign Solid Renal Lesions from Malignant Lesions Using Dual-Energy CT. J Med Assoc Thai 2022;105:413-22.

DOI: 10.35755/jmedassocthai.2022.05.13308

Knowledge of the RCC tumor subtypes is crucial because the different subtypes have different prognoses and treatment options. Therefore, researchers have attempted to differentiate the tumor subtypes according to their imaging features. Studies suggested that the degree of tumor enhancement may be associated with the subtypes of renal tumors. Studies by Kim et al[17], Hert et al[18], and Jinzaki et al[19] found that a hypervascular pattern can differentiate clear cell RCC from non-clear cell tumors, but that chromophobe and papillary RCCs could not be differentiated. However, a study by Sheir et al found a hypervascular pattern in only 49% of the clear cell subtypes, compared with 15% of papillary and 4% of chromophobe subtypes[20]. These findings imply that diagnosis of renal masses and renal tumor subtypes remains difficult.

In recent years, the advanced CT technology of dual-energy CT has been increasingly used to expand diagnostic performance over that of the conventional single-energy CT. By using two different X-ray spectra, different materials with similar CT numbers but differences in photon absorption can be differentiated. Dual-energy CT provides not only the routine anatomical images of conventional single-energy CT, but also the potential to analyze and quantify material composition through material-specific images, such as atomic number and iodine material density images[21-23]. Material-specific quantification can be performed on dual-energy CT data acquired in a single contrast-enhanced phase, which can contribute to reducing the radiation dose by as much as 30% to 50% in comparison with multiphase CT[24]. Furthermore, dual-energy CT may eliminate the pseudoenhancement effect by decreasing the beam-hardening artifacts related to iodine[25].

In a systematic review and meta-analysis to determine the diagnostic accuracy of quantitatively measured dual-energy CT iodine concentration in patients with renal masses, the pooled sensitivity and specificity of dual-energy CT in comparison with a reference standard of histologic analysis and another imaging technique over a period of at least 12-months were 96.6% (95% CI 85.9 to 99.3) and 95.1% (95% CI 90.7 to 97.5), respectively[24]. Although no differences in accuracy between the dual-energy CT and the conventional CT were identified, the meta-analysis was limited by the small number of the studies, with only 367 patients from five studies being eligible.

The purpose of the present study was to assess the ability of quantitative effective atomic number (Z_{eff}) and iodine density for differentiating malignant solid renal tumors from ambiguous benign lesions, and for differentiating the subtypes of RCC. Histopathologic analysis and follow-up imaging were used as the reference standards.

Materials and Methods

The present retrospective study was approved by the authors' Institutional Review Board (COA MURA2020/798) and the requirement for informed consent was waived. To accrue the patients, the present study institution's radiology information system (RIS) database was searched for patients that underwent dual-energy CT imaging of the abdomen on a Philips IQon Spectral CT scanner at the hospital between January 2017 and June 2020. The search terms included were "renal mass", "renal lesion", "partial nephrectomy", "total nephrectomy", "pathology", "renal biopsy", "clear cell", "renal cell carcinoma", "RCC", "lipid-poor angiomyolipoma", and "oncocytoma".

Potential subjects had at least one renal lesion of any size with either pathological diagnosis or a follow-up CT or magnetic resonance imaging (MRI) at least 24 months after the first study. The imaging study must have included a portal venous phase with a spectral base image series (SBI) available for post-processing.

Patients were excluded if there were no renal lesions identified on CT, a contrast-enhanced phase was absent, or no SBI series was available to construct the material-specific images. Renal lesions were excluded if there was evidence of macroscopic fat on an unenhanced image such as HU of −20 or less, no pathological confirmation, or no imaging follow-up (Figure 1).

Data collection

Patient demographics, clinical data, and indications for imaging were collected from the electronic medical records (EMR) and reviewed. For pathological data, the numbers and sizes of lesions were collected from pathological reports. A case with questionable lesions was discussed in consultation with the attending pathologist.

CT scanning technique

All examinations were performed on a dual-energy CT scanner (IQon spectral CT, Phillips Healthcare, Best, the Netherlands). The imaging was acquired using 120 kVp and automated tube current. The imaging data were reconstructed at 2.0

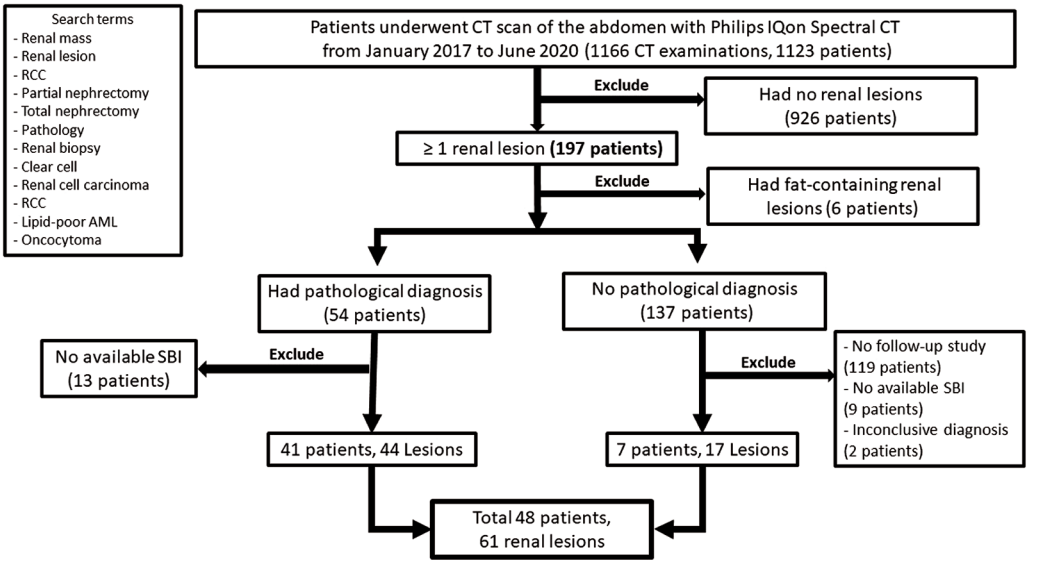

Figure 1. Flowchart showing the study population accrual process from target population to final study cohort.

to 3.0 mm slice thickness, depending on the type of study, with no intersectional gap. All patients were administered 75 to 100 mL of variable non-ionic iodinated contrast material with a concentration of 300 mg I/mL (Iopromide: Ultravist 300, Bayer Healthcare Pharmaceutical, Whippany, NJ, US; Ioversol: Optiray 300, Guerbet, Villepinte, France; and Iohexal: Omnipaque, GE Healthcare, Boston, MA, US) using a dual-chamber power injector at a flow rate of 2.5 to 3.5 mL/second. A bolus tracking technique was used to start the diagnostic scan after the contrast injection. The region of interest (ROI) for bolus tracking was set in the aorta at a level just above the diaphragm, with a trigger threshold level of 170 HU. The portal venous phase was obtained 30 to 40 seconds after the arterial phase, or 75 to 80 seconds after injection. All protocols included at least the top to the lower parts of both kidneys. The CT images were loaded into a picture archiving communication system (PACS). Z_{eff} and iodine maps were created using post-processing with Philips IntelliSpace portal software.

Analysis of CT images

Two observers, a third-year radiology resident and a CT technologist with18 years of experience, independently performed all measurements on the spectral images reconstructed with Philips IntelliSpace portal software. CT attenuation values, Z_{eff}, and iodine density were determined by drawing a circular ROI on an axial-section Z_{eff} dual-energy map of each renal lesion. ROIs of the same sizes were automatically placed at the same position of the renal lesion on conventional and iodine material density images (Figure 2, 3). For homogeneous lesions, the ROI included as much of the renal lesion as possible while avoiding the border of the mass. For heterogeneous or complex cystic lesions, the largest possible ROI was placed on the portion of visible high attenuation while avoiding calcification and the border of the lesion.

The CT attenuation, Z_{eff}, and iodine density results were recorded. To minimize variations in reviewer performance, an initial training session was performed on defining the area of interest. All measurements were repeated three times for each observer and the mean values of CT attenuation, Z_{eff}, and iodine density were calculated. The largest diameter of each lesion was measured on the axial contrast-enhanced conventional imaging.

Statistical analysis

Continuous variables were reported as mean ± standard deviation (SD). Categorial data were reported as number. Student's t-tests were used to compare the mean values of CT attenuation, Z_{eff}, and iodine density between the two types of renal lesions. The Fisher's exact test was used to determine whether there was a significant difference between the two types of renal lesions. Receiver operating characteristics (ROC) curve analysis was used to optimize cut-off values. The authors applied likelihood ratio for each distinct score value from ROC curve analysis. Interobserver agreement between the two observers was analyzed using Bland-Altman plots, with values of less than

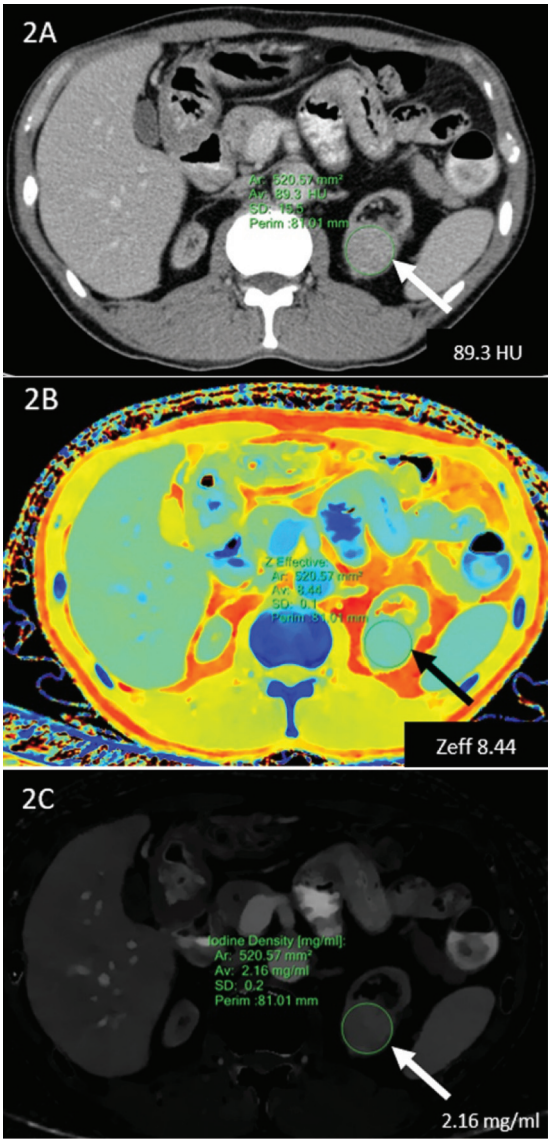

Figure 2. A 50-year-old man with pathologically-proven clear cell renal cell carcinoma in the left kidney (white arrow in A and C, black arrow in B). The axial portal venous phase conventional CT image in (2A) shows a homogeneous enhancing tumor in the left kidney with a CT attenuation value of 89.3 HU. On the dual-energy effective atomic number map (2B) and iodine density map (2C), the quantitative values obtained from circular ROI measurements showed mean Z_{eff} of 8.44 and iodine density of 2.16 mg/mL, respectively.

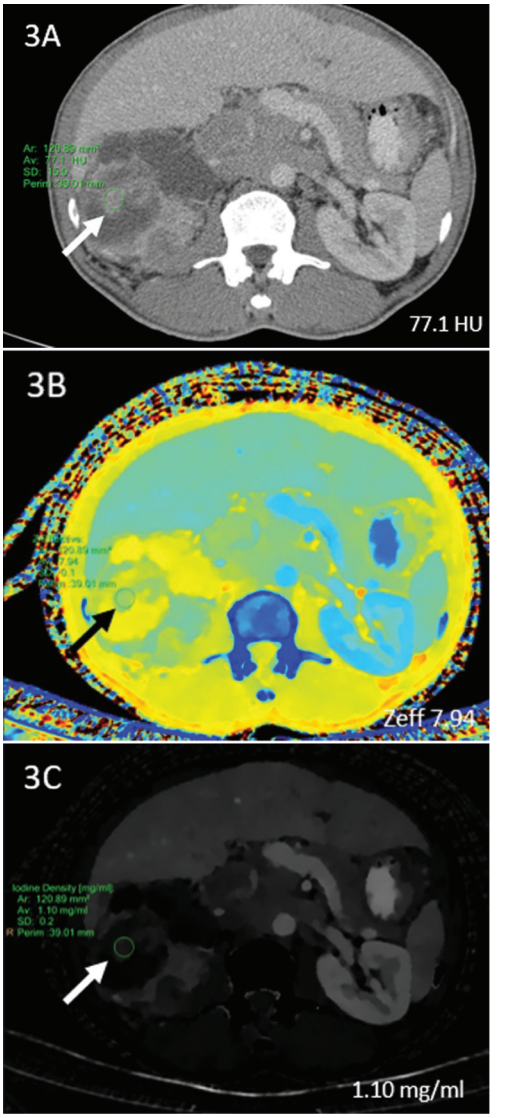

Figure 3. Example of ROI measurement in a heterogeneous renal lesion. A 56-year-old man with pathological-proven papillary cell renal cell carcinoma of the right kidney (white arrow in A and C, black arrow in B). The portal venous phase axial conventional CT image (3A) shows a heterogeneous mass in the right kidney (white arrow). The ROI was placed on the portion showing visible high attenuation with CT attenuation of 77.1 HU (3A). On the dual-energy effective atomic number (3B) and iodine density maps (3C), the quantitative values of Z_{eff} and iodine density were 7.94 and 1.10 mg/mL, respectively.

0.5, 0.5 to 0.75, 0.75 to 0.9, and more than 0.90 being taken to indicate poor, moderate, good, and excellent reliability, respectively[26].

Results

Renal masses

The original data search retrieved 1,166 CT examinations from 1,123 patients. After reviewing the studies, 926 patients were excluded because of no renal lesion being identified on the imaging studies. One hundred ninety-seven patients who had at least one renal lesion were identified, but six of these patients were excluded because their renal lesion contained fat. Among the 197 patients with at least one

Table 1. Patient demographics and lesion characteristics

Demographic data	Benign	Malignant	p-value
Sex; no. of patients			
Male/female	5/10	25/8	
Age (years); mean±SD	55±14.53	59±13.53	0.373
Location; no. of patients			
Right	8	16	
Left	7	17	
Size; no. of lesions			
<40 mm	25	23	
≥40 mm	2	11	
Mean±SD	19.81±10.46	37.73±29.90	0.026*

SD=standard deviation

* p<0.05, statistically significant

renal lesion, 54 patients had pathologic data, but the SBI necessary for post processing was not available for 13. Thus, 41 patients with a total of 44 renal histologically diagnosed lesions were included in the present study. Eleven of these lesions were confirmed by core needle biopsy, eight by wedge resection, two by nephroureterectomy, 22 by radical nephrectomy, and one by cyst deroofing.

Among the 137 patients who did not have pathological data, 130 were excluded for the following reasons, no follow-up imaging studies (n=119), no available SBI series for post-processing (n=9), and inconclusive diagnosis on follow-up imaging (n=2). The remaining seven patients with 17 lesions, had both follow-up imaging studies and available SBI series, were included in the present study. On the follow-up studies of these 17 lesions, three were stable, four were not visualized, and nine lesions had imaging characteristics of a benign lesion such as hyperdense cyst and fluid-attenuation. One subject was diagnosed with lymphoma by tissue diagnosis from the parotid region, and the renal lesion was lymphoma. The mean follow-up period was 26 months. Finally, sixty-one renal lesions from 48 patients were included in the present study (Figure 1). The demographics of these patients are shown in Table 1.

Among the 61 renal lesions, 34 were classified as malignant with 25 RCC, 9 other malignant tumors, and 27 benign lesions. The RCC subtypes included clear cell carcinoma (n=18), papillary cell RCC (n=4), chromophobe RCC (n=1), and non-specific RCC (n=2). The other malignant tumors included squamous cell carcinoma (n=1), urothelial carcinoma (n=4), metastasis from hemangiopericytoma (n=1), lymphoma (n=1), liposarcoma (n=1), and unspecified malignant (n=1). The benign lesions were adult

Table 2. Summary of renal lesion diagnoses based on histopathological data, clinical data, and imaging features

Lesion diagnosis	Number of lesions
Benign lesions (n=27)	
ADPKD	2
Acquired cystic disease	1
Simple cyst	2
Lipid-poor angiomyolipoma	17
Oncocytoma	2
Normal parenchyma	1
Focal pyelonephritis	1
Unspecific benign	1
Malignancy lesions (n=34)	
Clear cell RCC	18
Papillary cell RCC	4
Chromophobe RCC	1
Squamous cell carcinoma	1
Urothelial cell carcinoma	4
Metastasis-hemangiopericytoma	1
Liposarcoma	1
Lymphoma	1
Non-specific type RCC	2
Unspecified malignant	1

ADPKD=adult polycystic kidney disease; RCC=renal cell carcinoma

polycystic kidney disease (n=2), acquired cystic renal disease (n=1), simple renal cyst (n=2), lipid-poor angiomyolipoma (n=17), oncocytoma (n=2), normal renal parenchyma (n=1), focal pyelonephritis (n=1), and unspecified benign (n=1). A summary of the renal lesion diagnoses based on histopathological data, clinical data, and imaging features is provided in Table 2.

Significant differences in size were found between the benign lesions and malignant renal lesions (p=0.026; Table 1). A size of 18.5 mm or larger was considered the optimal threshold for defining malignant renal tumors, with a sensitivity of 82.35% and specificity of 55.56%.

Z_{eff}, iodine density, and CT attenuation

No significant differences were observed in Z_{eff}, iodine density, and CT attenuation between the benign lesions and the malignant renal tumors, nor between angiomyolipoma and RCC.

Among the malignant renal lesions, there were significant differences in Z_{eff}, iodine density, and CT attenuation between the RCCs and the other non-RCC malignant tumors (Z_{eff} at 8.44±0.09 versus 8.05±0.19, p=0.027, iodine at 2.25±0.98 versus 1.35±0.34, p=0.017, and CT attenuation at 97.62±24.32 versus

Table 3. Comparisons of effective atomic number, iodine density, and CT attenuation between different solid renal tumors

Type of renal tumor (n)	Effective atomic number (Z_{eff})		Iodine density (mg/mL)		CT attenuation (HU)	
	Mean±SD	p-value	Mean±SD	p-value	Mean±SD	p-value
Benign lesions (27)	8.33±0.52	0.983	2.12±1.14	0.615	89.53±45.10	0.384
Malignant lesions (34)	8.32±0.45		1.98±0.97		89.86±25.40	
Angiomyolipoma (17)	8.38±0.46	0.681	2.125±0.90	0.683	96.13±45.38	0.891
RCC (25)	8.44±0.09		2.25±0.98		97.62±24.32	
RCC (25)	8.44±0.09	0.027*	2.25±0.98	0.017*	97.62±24.32	0.006*
Non-RCC (8) (not included unspecified malignant)	8.05±0.19		1.35±0.34		70.91±11.63	
Clear cell RCC (18)	8.55±0.45	0.081	2.42±0.97	0.067	102.91±24.06	0.045*
Non-clear cell RCC (5) (not included non-specific RCC)	8.11±0.47		1.49±0.91		78.14±17.60	
Clear cell RCC (18)	8.55±0.45	0.036*	2.42±0.97	0.032*	102.91±24.06	0.001*
Papillary cell RCC (4)	8.01±0.39		1.28±0.71		72.66±15.34	

RCC=renal cell carcinoma; CT=computed tomography; SD=standard deviation

* p<0.05, statistically significant

Table 4. Accuracy of effective atomic number, iodine density, and CT attenuation in the diagnosis of renal cell carcinoma

Parameter	Threshold	Sensitivity (95% CI)	Specificity (95% CI)	PPV (95% CI)	NPV (95% CI)	Accuracy (95% CI)
Effective atomic number (Z_{eff})	8.22	76 (54.9 to 90.6)	75 (34.9 to 96.8)	90.5 (69.6 to 98.8)	50 (21.1 to 78.9)	75.8 (55.7 to 88.9)
Iodine density (mg/mL)	1.71	76 (54.9 to 90.6)	87.5 (47.3 to 99.7)	95 (75.1 to 99.9)	53.8 (25.1 to 80.8)	78.8 (61.09 to 91.0)
CT attenuation (HU)	79.50	80 (59.3 to 93.2)	87.5 (47.3 to 99.7)	95.2 (76.2 to 99.9)	58.3 (27.7 to 84.8)	81.8 (65.5 to 93.0)

CT=computed tomography; PPV=positive predictive value; NPV=negative predictive value; CI=confidence interval

70.91±11.63, p=0.006).

There was a borderline statistically significant difference in CT attenuation between clear cell RCC and non-clear cell RCC subtypes (102.91±24.06 HU versus 78.14±17.60 HU, p=0.045).

There were significant differences in Z_{eff}, iodine density, and CT attenuation between the clear cell RCC and the papillary RCC (Z_{eff} at 8.55±0.45 versus 8.01±0.39, p=0.036, iodine density at 2.42±0.97 versus 1.28±0.71, p=0.032, and CT attenuation at 102.91±24.06 versus 72.66±15.34, p=0.001). Comparisons of the quantitative measurements of renal lesions were shown in Table 3.

For Z_{eff}, the authors applied LR+=3 as the appropriate cutoff, which gave highest sensitivity and specificity. The ROC curve demonstrated that a Z_{eff} value of 8.22 was the optimal diagnostic threshold for discriminating the RCC group from the other malignant lesions, with sensitivity, specificity, and overall diagnostic accuracy of 76%, 75%, and 75.8%, respectively.

For iodine density, the authors applied LR+=6 as the appropriate cutoff. A value of 1.71 mg/mL was the optimal threshold for discriminating the RCC group from the other malignant tumors, with sensitivity, specificity, and overall diagnostic accuracy of 76%, 87.5%, and 78.8%, respectively.

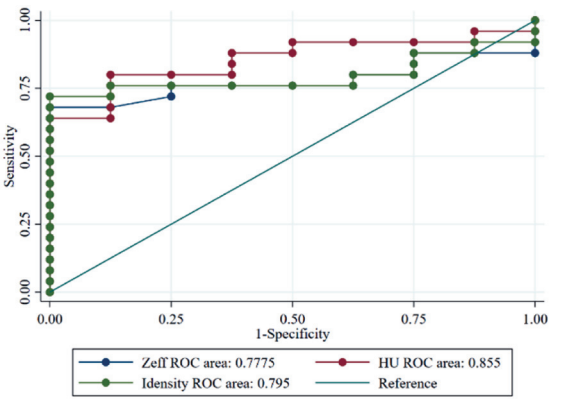

Figure 4. Receiver operating characteristics (ROC) curves for effective atomic number (Z_{eff}), CT attenuation, and iodine density. The optimal cutoff values for distinguish RCC from other malignant tumors (non-RCC) were 8.22 for Z_{eff}, 1.71 mg/mL for iodine density, and 79.5 HU for CT attenuation, with areas under the curve (AUCs) of 0.778 (95% CI 0.622 to 0.933), 0.795 (95% CI 0.643 to 0.947), and 0.855 (95% CI 0.725 to 0.985), respectively.

For CT attenuation, the authors applied LR+=6.4 as the appropriate cutoff. The optimal CT attenuation threshold for differentiating the RCC group from the other malignant tumors was 79.5 HU, with sensitivity, specificity, and overall diagnostic accuracy of 80%, 87.5%, and 81.8%, respectively. Details of

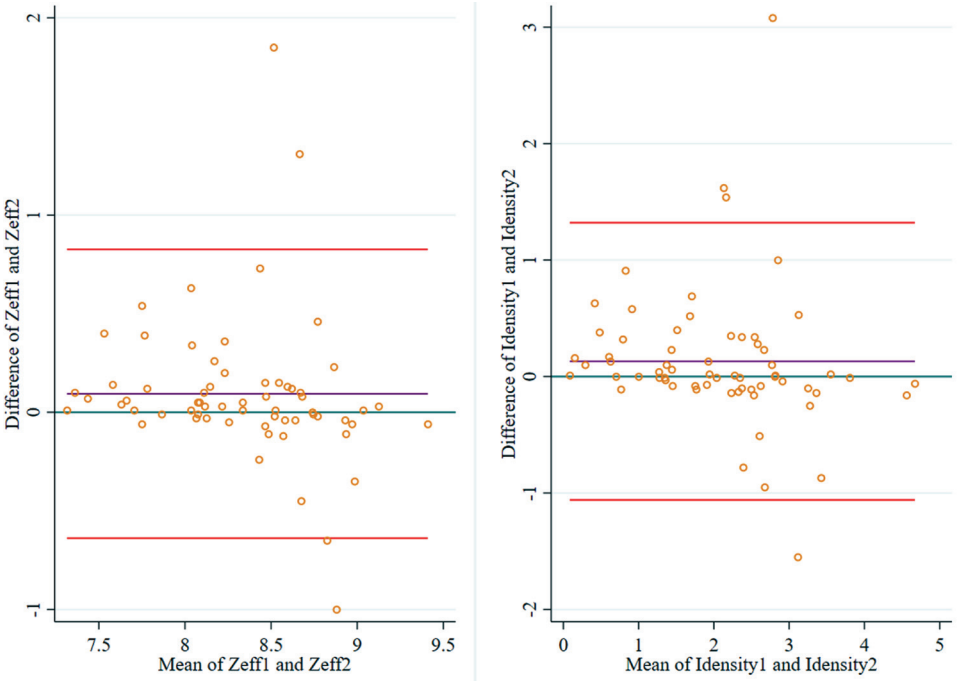

Figure 5. Bland-Altman plots showing the differences between the two readers in the measurement of effective atomic number (Z_{eff}) and iodine density.

the diagnostic accuracy with the use of the optimal thresholds for Z_{eff}, iodine density, and CT attenuation are summarized in Figure 4 and Table 4.

Interobserver agreement

The concordance correlation coefficients (CCCs) between the two readers for measuring Z_{eff}, iodine density, and CT attenuation were 0.72 (95% CI 0.60 to 0.84), 0.84 (95% CI 0.76 to 0.91), and 0.75 (95% CI 0.64 to 0.84), respectively (Figure 5). According to the CCCs(26), there was moderate inter-reader reliability (0.5 to 0.75) in the measurement of Z_{eff} and attenuation, and good reliability (0.75 to 0.9) in the measurement of iodine density.

Discussion

Significant differences in size were found between the benign and malignant solid renal lesions, with a mean size of 20 mm for the benign lesions and 38 mm for malignant lesions. Furthermore, 84.6% (11/13) of the lesions that were 4 cm or more were malignant, and a size of 18.5 mm or larger was considered an optimal threshold for diagnosing malignant renal tumors, with a sensitivity of 82.35% and specificity of 55.56%. A prior study also suggested that lesions with a size smaller than 40 mm tend to be benign[27].

The authors found that Z_{eff}, iodine density, and CT attenuation cannot be used to differentiate between benign lesions and malignant renal tumors, nor between RCC and lipid-poor angiomyolipoma. Nevertheless, Z_{eff}, iodine density, and CT attenuation showed significant differences between RCC and non-RCC, and between clear cell RCC and papillary RCC. The measurements from RCCs were higher than those from non-RCCs, and the measurements from clear cell RCCs were higher than those from papillary RCCs. Similarly, previous studies reported that iodine concentration quantified by dual energy CT was significantly higher in clear cell RCC than in papillary RCC[28,29], and that clear cell RCC enhances more and has a more heterogeneous appearance than other histologic subtypes[30,31]. However, the cut-off values of iodine density to differentiate clear cell and papillary RCCs, which were reported by different investigators were variable. The optimal threshold of iodine density reported by Mileto et al and Udare et al to discriminate between clear cell and papillary RCCs was 0.9 mg/mL and 2.5 mg/mL, respectively[28,29]. Whereas, Marcon et al found that a cutoff value of 3.1 mg/mL of iodine density could distinguish between papillary and clear cell RCCs with an accuracy of 86.8%[32]. These disparities could be attributed to different CT scanner vendors, contrast administration rates, and study phases.

For the differentiation between RCC and the other non-RCC malignant tumors, the present study analyses demonstrated optimal thresholds of 8.22, 1.71 mg/mL, and 79.50 HU for Z_{eff}, iodine density, and CT attenuation, respectively, with sensitivities of 76%, 76%, and 80%, respectively.

The authors observed that the accuracy obtained using an optimal conventional CT attenuation threshold (81.82%) for differentiating RCC from other solid renal tumors was slightly higher than those obtained with either Z_{eff} (75.8%) or iodine density (78.8%). These findings imply that neither dual-energy Z_{eff} nor iodine density alone is superior to conventional CT attenuation in the discrimination of RCC from other solid renal tumors. However, the dual-energy material-specific images may be used as an adjunct to conventional CT and may assist the radiologist in the evaluation of a renal lesion.

The mean attenuation value of clear cell RCC was higher than that of non-clear cell RCC at 102.91±24.06 HU versus 78.14±17.60 HU (p=0.045), although with only borderline significance. It should not be used as an isolated diagnostic value to diagnose clear cell RCC, and the authors, did not, therefore calculate an optimal cutoff threshold for CT attenuation. However, the authors found no significant differences in Z_{eff} and iodine density between clear cell and non-clear cell RCC, in contrast to the study by Mileto et al, which found that the mean Z_{eff} of clear cell RCC was significantly higher than that of non-clear cell RCC at 9.9±0.68 versus 8.64±0.48[33]. The authors found no significant differences in Z_{eff}, iodine density, or CT attenuation between lipid-poor angiomyolipoma and RCC, which differed from a previous study by Wan et al[34]. In their study, the Z_{eff} of a RCC group was lower than that of a lipid-poor angiomyolipoma group. The different results may be a consequence of differences in the patient selection criteria and phases of contrast-enhanced CT. Wan et al used a corticomedullary phase, as opposed to the portal venous phase used in the present study. These results suggested that more research into quantitative assessments of dual-energy Z_{eff} and iodine density for differentiating types of renal lesions is needed.

A major limitation of the present study is the small sample size, which resulted from the short recruitment period, due to the Phillips IQon Spectral CT scanner being recently installed in January 2017. The small number of benign lesions compared with the number of malignant lesions might have limited the statistical sensitivity of the present study. Furthermore, the portal venous phase SBI series required to measure Z_{eff} and iodine density were not available for some suitable patients. Another limitation is that tumors considered most likely to be benign did not undergo further tissue biopsy or nephrectomy. Therefore, there were only a small number of benign tumors with pathological diagnoses, even though tissue diagnosis is considered the reference standard. However, among those without pathological confirmation, the authors included those with follow-up imaging of at least two years to confirm stability. Another limitation is the retrospective design of the study. In cases with large heterogeneous, infiltrative, or multiple lesions, it was uncertain whether the lesion measured on CT imaging exactly matched the biopsy tissue subjected to histological analysis. If multiple lesions were present in the pathological specimen, the tissue might have been sampled randomly, if the lesions had the same histopathological components. As this was a retrospective study, it was not possible to inform the surgeons and pathologists about the specific location of the concerned lesion prior to operation.

Conclusion

The present study found no significant differences in Z_{eff}, iodine density, or CT attenuation between benign and malignant solid renal tumors. The Z_{eff} and iodine maps constructed from dual-energy CT may not be used alone to differentiate benign from malignant solid renal tumor, but they have potential diagnostic value in differentiating RCC from other malignant renal tumors, clear cell RCC from non-clear cell RCC, and clear cell RCC from papillary cell RCC. The authors suggest that future prospective studies with sufficient sample size hold promise for better outcomes, higher accuracy, and new valuable findings of clinical relevance for radiologists in the noninvasive differentiation of malignant renal lesions from ambiguous benign lesions and the discrimination of RCC subtypes.

What is already known on this topic?

Some types of benign renal lesions such as lipid-poor angiomyolipoma and oncocytoma have imaging features that overlap with those of renal cell carcinoma. Previous studies reported that the lipid-poor angiomyolipoma had a significantly higher mean attenuation value compared with that of clear cell RCC on unenhanced CT scans. However, this observation is not consistent.

Dual-energy CT provides not only the routine anatomical images of conventional single-energy CT, but also the potential to analyze and quantify material

composition through material-specific images, such as atomic number and iodine material density images.

What this study adds?

This study found that Z_{eff}, iodine density, and CT attenuation cannot be used to differentiate between benign lesions and malignant renal tumors, nor between RCC and lipid-poor angiomyolipoma. Nevertheless, Z_{eff}, iodine density, and CT attenuation showed significant differences between RCC and non-RCC, and between clear cell RCC and papillary RCC. The measurements from RCCs were higher than those from non-RCCs, and the measurements from clear cell RCCs were higher than those from papillary RCCs.

The optimal thresholds for Z_{eff}, iodine density, and CT attenuation for distinguishing RCC from other malignant tumors were 8.22, 1.71 mg/mL, and 79.50 HU, respectively, which provided sensitivity of 76%, 76%, and 80%, respectively.

The accuracy obtained using an optimal conventional CT attenuation threshold (81.82%) for differentiating RCC from other solid renal tumors was slightly higher than those obtained with either Z_{eff} (75.8%) or iodine density (78.8%).

Acknowledgement

The authors are grateful to Ms. Sukanya Siriyotha, who contributed to the statistical applications in this research. The authors are also grateful to the radiology technicians at AIMC (Advance IMaging Center), Ramathibodi Hospital, who provided valuable information about the imaging techniques and post-processed the dual-energy CT imaging used in this article.

Conflicts of interest

The authors declare no conflict of interest.

References

1. Hollingsworth JM, Miller DC, Daignault S, Hollenbeck BK. Rising incidence of small renal masses: a need to reassess treatment effect. J Natl Cancer Inst 2006;98:1331-4.
2. Leone AR, Diorio GJ, Spiess PE, Gilbert SM. Contemporary issues surrounding small renal masses: Evaluation, diagnostic biopsy, nephron sparing, and novel treatment modalities. Oncology (Williston Park) 2016;30:507-14.
3. Herts BR, Silverman SG, Hindman NM, Uzzo RG, Hartman RP, Israel GM, et al. Management of the incidental renal mass on CT: A white paper of the ACR Incidental Findings Committee. J Am Coll Radiol 2018;15:264-73.
4. Silverman SG, Mortele KJ, Tuncali K, Jinzaki M, Cibas ES. Hyperattenuating renal masses: etiologies, pathogenesis, and imaging evaluation. Radiographics 2007;27:1131-43.
5. Krishna S, Murray CA, McInnes MD, Chatelain R, Siddaiah M, Al-Dandan O, et al. CT imaging of solid renal masses: pitfalls and solutions. Clin Radiol 2017;72:708-21.
6. Vos N, Oyen R. Renal angiomyolipoma: The good, the bad, and the ugly. J Belg Soc Radiol 2018;102:41.
7. Thiravit S, Teerasamit W, Thiravit P. The different faces of renal angiomyolipomas on radiologic imaging: a pictorial review. Br J Radiol 2018;91:20170533.
8. Simpfendorfer C, Herts BR, Motta-Ramirez GA, Lockwood DS, Zhou M, Leiber M, et al. Angiomyolipoma with minimal fat on MDCT: can counts of negative-attenuation pixels aid diagnosis? AJR Am J Roentgenol 2009;192:438-43.
9. Xie P, Yang Z, Yuan Z. Lipid-poor renal angiomyolipoma: Differentiation from clear cell renal cell carcinoma using wash-in and washout characteristics on contrast-enhanced computed tomography. Oncol Lett 2016;11:2327-31.
10. Jinzaki M, Tanimoto A, Narimatsu Y, Ohkuma K, Kurata T, Shinmoto H, et al. Angiomyolipoma: imaging findings in lesions with minimal fat. Radiology 1997;205:497-502.
11. Zhang YY, Luo S, Liu Y, Xu RT. Angiomyolipoma with minimal fat: differentiation from papillary renal cell carcinoma by helical CT. Clin Radiol 2013;68:365-70.
12. Chenam A, Lau C. Management of small renal masses. Cancer Treat Res 2018;175:105-26.
13. Woo S, Cho JY. Imaging findings of common benign renal tumors in the era of small renal masses: differential diagnosis from small renal cell carcinoma: current status and future perspectives. Korean J Radiol 2015;16:99-113.
14. Warren AY, Harrison D. WHO/ISUP classification, grading and pathological staging of renal cell carcinoma: standards and controversies. World J Urol 2018;36:1913-26.
15. Muglia VF, Prando A. Renal cell carcinoma: histological classification and correlation with imaging findings. Radiol Bras 2015;48:166-74.
16. Padala SA, Barsouk A, Thandra KC, Saginala K, Mohammed A, Vakiti A, et al. Epidemiology of renal cell carcinoma. World J Oncol 2020;11:79-87.
17. Kim JK, Kim TK, Ahn HJ, Kim CS, Kim KR, Cho KS. Differentiation of subtypes of renal cell carcinoma on helical CT scans. AJR Am J Roentgenol 2002;178:1499-506.
18. Herts BR, Coll DM, Novick AC, Obuchowski N, Linnell G, Wirth SL, et al. Enhancement characteristics of papillary renal neoplasms revealed on triphasic helical CT of the kidneys. AJR Am J Roentgenol 2002;178:367-72.
19. Jinzaki M, Tanimoto A, Mukai M, Ikeda E, Kobayashi S, Yuasa Y, et al. Double-phase helical CT of small

renal parenchymal neoplasms: correlation with pathologic findings and tumor angiogenesis. J Comput Assist Tomogr 2000;24:835-42.
20. Sheir KZ, El-Azab M, Mosbah A, El-Baz M, Shaaban AA. Differentiation of renal cell carcinoma subtypes by multislice computerized tomography. J Urol 2005;174:451-5.
21. Patino M, Prochowski A, Agrawal MD, Simeone FJ, Gupta R, Hahn PF, et al. Material separation using dual-energy CT: current and emerging applications. Radiographics 2016;36:1087-105.
22. Silva AC, Morse BG, Hara AK, Paden RG, Hongo N, Pavlicek W. Dual-energy (spectral) CT: applications in abdominal imaging. Radiographics 2011;31:1031-46; discussion 47-50.
23. Kaza RK, Ananthakrishnan L, Kambadakone A, Platt JF. Update of dual-energy CT applications in the genitourinary tract. AJR Am J Roentgenol 2017;208:1185-92.
24. Mileto A, Nelson RC, Paulson EK, Marin D. Dual-energy MDCT for imaging the renal mass. AJR Am J Roentgenol 2015;204:W640-7.
25. Schabel C, Patel B, Harring S, Duvnjak P, Ramírez-Giraldo JC, Nikolaou K, et al. Renal lesion characterization with spectral CT: Determining the optimal energy for virtual monoenergetic reconstruction. Radiology 2018;287:874-83.
26. Koo TK, Li MY. A guideline of selecting and reporting intraclass correlation coefficients for reliability research. J Chiropr Med 2016;15:155-63.
27. van Oostenbrugge TJ, Fütterer JJ, Mulders PFA. Diagnostic imaging for solid renal tumors: A pictorial review. Kidney Cancer 2018;2:79-93.
28. Mileto A, Marin D, Alfaro-Cordoba M, Ramirez-Giraldo JC, Eusemann CD, Scribano E, et al. Iodine quantification to distinguish clear cell from papillary renal cell carcinoma at dual-energy multidetector CT: a multireader diagnostic performance study. Radiology 2014;273:813-20.
29. Udare A, Walker D, Krishna S, Chatelain R, McInnes MD, Flood TA, et al. Characterization of clear cell renal cell carcinoma and other renal tumors: evaluation of dual-energy CT using material-specific iodine and fat imaging. Eur Radiol 2020;30:2091-102.
30. Young JR, Margolis D, Sauk S, Pantuck AJ, Sayre J, Raman SS. Clear cell renal cell carcinoma: discrimination from other renal cell carcinoma subtypes and oncocytoma at multiphasic multidetector CT. Radiology 2013;267:444-53.
31. Low G, Huang G, Fu W, Moloo Z, Girgis S. Review of renal cell carcinoma and its common subtypes in radiology. World J Radiol 2016;8:484-500.
32. Marcon J, Graser A, Horst D, Casuscelli J, Spek A, Stief CG, et al. Papillary vs clear cell renal cell carcinoma. Differentiation and grading by iodine concentration using DECT-correlation with microvascular density. Eur Radiol 2020;30:1-10.
33. Mileto A, Allen BC, Pietryga JA, Farjat AE, Zarzour JG, Bellini D, et al. Characterization of incidental renal mass with dual-energy CT: Diagnostic accuracy of effective atomic number maps for discriminating nonenhancing cysts from enhancing masses. AJR Am J Roentgenol 2017;209:W221-30.
34. Wan Y, Guo H, Ji L, Li Z, Gao J. Gemstone spectral imaging dual-energy computed tomography for differentiation of renal cell carcinoma and minimal-fat renal angiomyolipoma. J Cancer Res Ther 2018;14 Suppl:S394-9.